Contribution from the Department of Chemistry,
Emory University, Atlanta, Georgia 30322

Molecular Structure of Bis[μ-5,5-dimethyl-1,3,2-dioxaphosphorinano]-hexacarbonyldiiron, $[\overline{OCH_2CMe_2CH_2OP}Fe(CO)_3]_2$

WALTER K. DEAN,* BARBARA L. HEYL, and DONALD G. VANDERVEER

Received September 2, 1977

Bis[μ-5,5-dimethyl-1,3,2-dioxaphosphorinano]-hexacarbonyldiiron, $[\overline{OCH_2CMe_2CH_2OP}Fe(CO)_3]_2$, crystallizes in the monoclinic space group $P2_1/c$ with four molecules in a unit cell with dimensions a = 7.884 (1) Å, b = 9.828 (6) Å, c = 29.282 (13) Å, and β = 91.60 (3)°. Full-matrix least-squares refinement of 2982 independent counter data yielded R = 0.034, R_w = 0.047. The molecule has the "butterfly" geometry typical of $[(\mu\text{-X})Fe(CO)_3]_2$ complexes. The detailed structure of the compound is discussed in relation to the stereochemical nonrigidity of the iron–phosphorus ring. There appears to be no indication of steric interaction between the phosphorinane rings which would distort the molecule so as to lower the barrier to Fe_2P_2 ring inversion, nor is there any apparent correlation between the electronegativity of the substituents on phosphorus (as reflected in the structural details of the molecule) and the degree of fluxionality of this and similar compounds.

Introduction

The synthesis and properties of bis[μ-5,5-dimethyl-1,3,2-dioxophosphorinano]-hexacarbonyldiiron, $[\overline{OCH_2CMe_2CH_2OP}Fe(CO)_3]_2$ (hereafter abbreviated as $[(\mu\text{-DMP})Fe(CO)_3]_2$) have been reported by Bartish and Kraihanzel.[1] This complex, which is the first example of a bridging phosphorinano complex, is unique in that it exhibits two different modes of proton site exchange; the high-temperature process (inversion of the Fe_2P_2 ring) exhibits a coalescence temperature somewhat lower than those of other reported $[(\mu\text{-}R_2P)Fe(CO)_3]_2$ complexes.

We have undertaken the determination of the structure of this compound in order to examine the structural properties of the phosphorinane ligand in a bridging role and to confirm the proposed structure on which the interpretation of its NMR spectrum was based, both as to the gross structure and as to the puckering and conformation of the phosphorinane rings. Also, we wished to look for structural features such as steric interaction between the phosphorinane rings which might account for the relative ease of inversion of the Fe_2P_2 ring. Finally, we wished to extend the relationship between the structural details of $[(\mu\text{-}R_2P)Fe(CO)_3]_2$ complexes and the electronegativity of the substituents on phosphorus, developed by Clegg[2] and Burdett[3] for molecules where R = H, CH_3, C_6H_5, and CF_3, to include an alkoxy-substituted bridging phosphide complex and to determine whether any correlation could be observed between the electronic properties of the bridging ligand and the ease of inversion of the Fe_2P_2 ring in compounds of this type.

Experimental Section

Collection of Intensity Data. A sample of $[(\mu\text{-DMP})Fe(CO)_3]_2$ was supplied by Dr. C. M. Bartish. Suitable crystals were obtained by slow evaporation of a dichloromethane–heptane solution of the compound. The crystal selected for data collection was a short, approximately hexagonal rod 0.75 mm long by 0.30 mm thick. It was mounted on a glass fiber with epoxy cement and was centered in a random orientation on a Syntex $P2_1$ automated four-circle diffractometer equipped with a graphite monochromator.

The observed systematic absences ($h0l$, l odd; $0k0$, k odd) determined the space group as monoclinic $P2_1/c$.

Further crystal, unit cell, and data collection data are presented in Table I.

The intensity data were corrected for Lorentz and polarization effects, using the form of the Lp factor given in eq 1. (This equation assumes that the monochromator crystal is 50% mosaic and 50% perfect; the monochromator angle $2\theta_m$ is 12.2° for Mo Kα radiation.) No corrections were made for absorption, in view of the small absorption coefficient and narrow range of transmission coefficients (see Table I). Standard deviations $\sigma(I)$ were assigned by the procedure of Doedens and Ibers,[4] using an "ignorance factor" p of 0.05. Of a total of 4014 independent data measured, 2982 were considered observed ($I \geq 3\sigma(I)$); only the observed data were used in the structure solution and refinement.

$$Lp = \frac{0.5}{\sin 2\theta}\left[\left(\frac{1+\cos^2 2\theta_m \cos^2 2\theta}{1+\cos^2 2\theta_m}\right) + \left(\frac{1+|\cos 2\theta_m|\cos 2\theta}{1+|\cos 2\theta_m|}\right)\right] \quad (1)$$

Table I. Details of Data Collection

A. Crystal Data

Formula	$Fe_2P_2O_{10}C_{16}H_{20}$	β, deg	91.60 (3)
Mol wt	545.97	V, Å^3	2268 (2)
Space group	$P2_1/c$	Z	4
a, Å (25 °C)	7.884 (1)[a]	ρ(obsd), g cm^{-3}	1.600
b, Å	9.828 (6)	ρ(calcd), g cm^{-3}	1.595[b]
c, Å	29.282 (13)		

B. Collection and Treatment of Intensity Data

Radiation	Mo Kα ($\bar{\lambda}$ 0.710 730 Å)
Monochromator angle, deg	12.2
Takeoff angle, deg	6.5
Reflections measd	$\pm h, +k, +l$
2θ range, deg	4–50
Scan type	θ(crystal)–2θ(counter)
Scan speed, deg/min	5.9
Scan range, deg	$[2\theta(K_{\alpha_1}) - 1.0] \rightarrow [2\theta(K_{\alpha_2}) + 1.0]$
Background measurement	At beginning and end of each scan, each for half of total scan time
Standards	3 every 100 reflections[c]
Absorption coeff, cm^{-1}	14.84
Estd range of transmission factors	0.90–0.96

[a] Based on a least-squares fit to the setting angles of the Mo K$\bar{\alpha}$ peaks of 15 reflections with 2θ = 8–21°. [b] Measured by neutral bouyancy in aqueous NaI. [c] Maximum deviations of intensities from their mean values were 2.4% for 060, 2.6% for 400, and 2.1% for 0,0,14.

Solution and Refinement of the Structure. The structure was solved by direct methods. Normalized structure factors (E's) were calculated using scale and overall temperature factors obtained from a Wilson plot. The 496 reflections with the highest E's were used as input to the program MULTAN. Reflections in the starting set were ($\bar{2}$,3,17), (5,1,18), (012), ($\bar{2}$,11,4), (2,3,13), and (6,1,10), with the first three being used for origin specification. An E map based on the phase set having the highest figure of merit clearly revealed the positions of the iron and phosphorus atoms. These four positions were then least-squares refined, and a Fourier map phased on the refined positions yielded coordinates for all remaining nonhydrogen atoms.

Refinement of the structure proceeded smoothly. After isotropic refinement of the nonhydrogen atoms, a difference Fourier synthesis showed all expected hydrogen atoms. The hydrogen atoms were held in fixed positions with fixed isotropic thermal parameters of B = 6.0 Å^2 during subsequent refinement. The final model included anisotropic thermal parameters for all nonhydrogen atoms (271 variable pa-

0020-1669/78/1317-1909$01.00/0

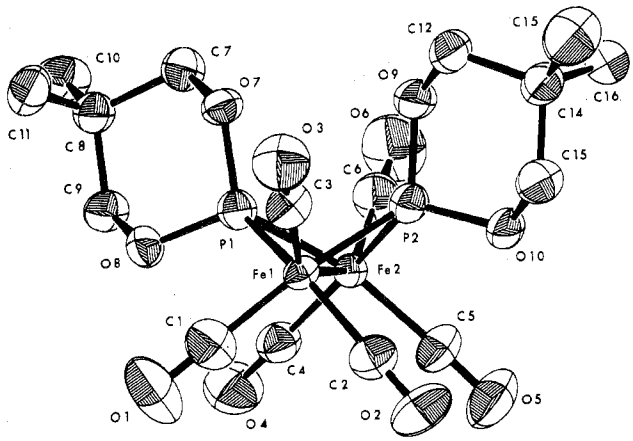

Figure 1. Structure of the $[(\mu\text{-DMP})Fe(CO)_3]_2$ molecule (50% probability ellipsoids).

rameters; data-to-parameter ratio 11.00:1). All full-matrix least-squares cycles were based on the minimization of $\sum w||F_o| - |F_c||^2$, where $w = \sigma(F_o)^{-2}$. The final discrepancy indices for the observed data were $R = 0.034$ and $R_w = 0.047$, and the "goodness of fit" (GOF) was 1.360. (These quantities are defined in eq 2–4; n is the number

$$R = \left[\frac{\Sigma||F_o| - |F_c||}{\Sigma|F_o|}\right] \quad (2)$$

$$R_w = \left[\frac{\Sigma w(|F_o| - |F_c|)^2}{\Sigma w|F_o|^2}\right]^{1/2} \quad (3)$$

$$\text{GOF} = \left[\frac{\Sigma w(|F_o| - |F_c|)^2}{n - v}\right]^{1/2} \quad (4)$$

of data and v is the number of variables.) The corresponding indices for all data were $R = 0.055$, $R_w = 0.057$, and GOF = 1.232. There were 86 reflections for which $||F_o| - |F_c|| > 3\sigma(F_o)$; these were almost all due to high background counts. An inspection of R, R_w, the fraction of data rejected as a function of parity, $(\sin\theta)/\lambda$, and Miller indices revealed no anomalies. The maximum electron density on a final difference Fourier synthesis was 0.31 e Å^{-3}. No parameter shifted by more than 0.4σ during the last refinement cycle.

The scattering factors of Cromer and Mann[5a] for neutral atoms were used throughout the analysis, with corrections for the real and imaginary components of anomalous dispersion for iron and phosphorus atoms.[5b] Computer programs used included local programs for data reduction and least-squares planes, as well as locally modified versions of Zalkin's FORDAP for Fourier maps, Ibers' NUCLSS refinement program, the Busing–Martin–Levy ORFFE function and error program, and Johnson's ORTEP plotting program.

The values of $|F_o|$ and $|F_c|$ (in electrons × 10) for all reflections used in the refinement are included as supplementary material. Final positional and thermal parameters for all atoms are presented in Table II. Interatomic distances, bond angles, and least-squares planes are given in Table III.

Results and Discussion

Description of the Structure. The structure of $[(\mu\text{-DMP})Fe(CO)_3]_2$ consists of discrete molecules, as depicted in Figure 1. All atoms are in general positions; however, the molecule has approximate C_2 symmetry with the pseudo-twofold axis passing through the midpoints of the Fe–Fe and P···P vectors.

The geometry of the Fe_2P_2 ring is typical of $[(\mu\text{-X})Fe(CO)_3]_2$ compounds, of which some 20 structures have now been reported. The Fe_2P_2 ring is puckered, with dihedral angles about the Fe–Fe bond of 108.5° and about the P···P vector of 106.6°.

The phosphorinane ring is also puckered and adopts a chair conformation. The rings are tilted with respect to the Fe–Fe axis, so that one iron atom is axial and the other is equatorial

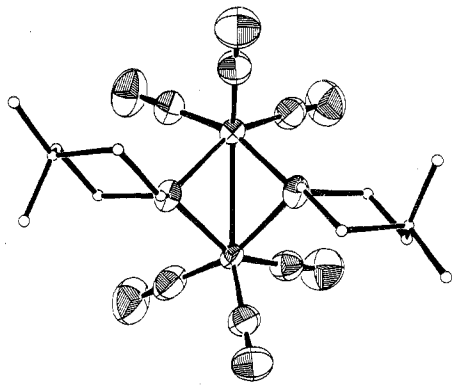

Figure 2. View of the $[(\mu\text{-DMP})Fe(CO)_3]_2$ molecule along its pseudo-twofold rotation axis, showing the conformation of the phosphorinane rings.

with respect to each ring; also, because of the approximate C_2 symmetry of the molecule, each iron atom is axial with respect to one ring and equatorial with respect to the other. (These relationships can best be seen in Figure 2, in which the phosphorinane ring carbon and oxygen atoms are represented as small circles in order to show the ring conformations more clearly.) This is a rather interesting result; it shows that the presence of two identical bulky $Fe(CO)_3$ substituents on the same atom of the phosphorinane ring does not, at least in the static structure, alter its conformational preference for having one clearly axial and one equatorial substituent; there is no tendency to distort the phosphorinane rings so as to make both iron atoms more nearly equivalent with respect to the rings.

Figure 2 also shows that the two PO_2 systems are nearly coplanar; the dihedral angle between the two PO_2 planes is 176.0°, and all of the atoms are within 0.065 Å of the common plane through both PO_2 systems (see Table III). One would expect that any steric interaction between the phosphorinane rings would result in a twisting of the two PO_2 planes with respect to one another in order to reduce interaction between the ring oxygen atoms. The presumptive conclusion is that steric repulsion between the rings is in fact rather small; this conclusion is supported by the observation that the O(7)···O(9) distance (3.075 Å) is only slightly smaller than the intermolecular contacts within the structure (the shortest of which are presented in Table III).

The details of the geometry of the Fe_2P_2 ring in $[(\mu\text{-DMP})Fe(CO)_3]_2$ are of interest as they relate to the electronegativity of the substituents on phosphorus. Clegg[2] has argued on the basis of hybridization and Burdett[3] has argued on molecular orbital grounds that increasing electronegativity of the substituents on phosphorus in $[R_2PFe(CO)_3]_2$ complexes leads to a smaller R–P–R angle and a larger Fe–P–Fe angle and that the Fe–Fe distance and the "flap angle" between the FeP_2 planes increase concomitantly; Burdett has demonstrated this effect for complexes where R = H, CH_3, C_6H_5, and CF_3. The detailed geometry of the Fe_2P_2 ring in $[(\mu\text{-DMP})Fe(CO)_3]_2$ is consistent with expectations based on a qualitative estimate of the electronegativity of an alkoxy group as intermediate between that of CF_3 and those of H, alkyl, and aryl groups (the phosphorinane ring in $[(\mu\text{-DMP})Fe(CO)_3]_2$ being considered as a phosphorus substituted by two alkoxy groups). As shown in Table IV, the relevant structural parameters in $[(\mu\text{-DMP})Fe(CO)_3]_2$ are generally intermediate between those of $[(CF_3)_2PFe(CO)_3]_2$ and $[R_2PFe(CO)_3]_2$ (R = H, CH_3, C_6H_5). The same trend is seen for the R–P–R angle in the series $(\mu\text{-}[p\text{-}MeC_6H_4]_2P)(\mu\text{-OH})Fe_2(CO)_6$ (103.4°),[6] $[(\mu\text{-DMP})Fe(CO)_3]_2$ (average 101.9°), and $[(CF_3)_2PFe(CO)_3]_2$ (96.6°).[2] The only exceptions are the Fe–P distances, which are shortest in $[(\mu\text{-DMP})Fe(CO)_3]_2$. This may reflect a greater degree of Fe–P $d\pi$–$d\pi$ bonding in the phosphorinane

Table II

Final Atomic Parameters[a]

Atom	x/a	y/b	z/c	Atom	x/a	y/b	z/c
Fe(1)	0.41346 (7)	0.30490 (6)	0.39965 (2)	C(12)	0.2742 (6)	−0.0974 (4)	0.3929 (2)
Fe(2)	0.09570 (7)	0.33996 (6)	0.36686 (2)	C(13)	0.1946 (6)	−0.1295 (4)	0.4387 (2)
P(1)	0.3309 (1)	0.3136 (1)	0.32929 (3)	C(14)	0.2127 (6)	−0.0048 (4)	0.4691 (1)
P(2)	0.1993 (1)	0.1623 (1)	0.39996 (3)	C(15)	0.3010 (9)	−0.2447 (6)	0.4603 (2)
O(1)	0.6083 (5)	0.5565 (4)	0.3867 (1)	C(16)	0.0091 (7)	−0.1698 (5)	0.4332 (2)
O(2)	0.3400 (5)	0.3792 (4)	0.4944 (1)	H(7-1)	0.1532	0.1918	0.2505
O(3)	0.6873 (4)	0.1077 (4)	0.4078 (1)	H(7-2)	0.3387	0.1144	0.2368
O(4)	0.0778 (5)	0.6192 (3)	0.3316 (1)	H(9-1)	0.3866	0.5290	0.2396
O(5)	−0.0864 (5)	0.4103 (4)	0.4499 (1)	H(9-2)	0.2036	0.4626	0.2586
O(6)	−0.1541 (6)	0.2054 (5)	0.3076 (1)	H(10-1)	0.2747	0.2727	0.1582
O(7)	0.3567 (4)	0.1881 (2)	0.2949 (1)	H(10-2)	0.2722	0.4415	0.1680
O(8)	0.3926 (3)	0.4407 (3)	0.2992 (1)	H(10-3)	0.1266	0.3649	0.1796
O(9)	0.1988 (4)	0.0221 (3)	0.3719 (1)	H(11-1)	0.5651	0.2366	0.1991
O(10)	0.1312 (4)	0.1140 (3)	0.4487 (1)	H(11-2)	0.6110	0.3037	0.2467
C(1)	0.5308 (6)	0.4602 (5)	0.3917 (2)	H(11-3)	0.5913	0.4016	0.1993
C(2)	0.3701 (6)	0.3493 (5)	0.4578 (2)	H(12-1)	0.2614	−0.1803	0.3781
C(3)	0.5798 (6)	0.1854 (4)	0.4041 (1)	H(12-2)	0.4282	−0.0681	0.3981
C(4)	0.0857 (6)	0.5118 (5)	0.3460 (1)	H(14-1)	0.3156	0.0144	0.4765
C(5)	−0.0178 (6)	0.3826 (5)	0.4178 (2)	H(14-2)	0.1273	−0.0134	0.4982
C(6)	−0.0564 (6)	0.2594 (5)	0.3309 (2)	H(15-1)	0.2834	−0.3357	0.4476
C(7)	0.2863 (6)	0.2019 (4)	0.2487 (1)	H(15-2)	0.2526	−0.2538	0.4910
C(8)	0.3580 (6)	0.3272 (4)	0.2246 (1)	H(15-3)	0.4429	−0.2125	0.4538
C(9)	0.3201 (5)	0.4527 (4)	0.2530 (1)	H(16-1)	−0.0018	−0.2465	0.4124
C(10)	0.2628 (8)	0.3435 (5)	0.1790 (2)	H(16-2)	−0.0387	−0.0970	0.4178
C(11)	0.5476 (7)	0.3127 (5)	0.2180 (2)	H(16-3)	−0.0486	−0.2137	0.4505

Anisotropic Thermal Parameters[b]

Atom	B_{11}	B_{22}	B_{33}	B_{12}	B_{13}	B_{23}
Fe(1)	3.05 (2)	3.05 (3)	2.40 (2)	0.21 (2)	−0.09 (2)	0.15 (2)
Fe(2)	2.98 (2)	2.80 (3)	2.57 (3)	0.10 (2)	−0.03 (2)	0.04 (2)
P(1)	3.43 (4)	2.49 (4)	2.20 (4)	0.17 (3)	0.12 (3)	0.21 (3)
P(2)	3.76 (5)	2.71 (4)	2.24 (4)	0.03 (4)	0.32 (3)	0.12 (3)
O(1)	8.9 (3)	5.6 (2)	7.2 (2)	−3.5 (2)	−1.8 (2)	1.7 (2)
O(2)	6.7 (2)	7.7 (2)	3.2 (2)	0.9 (2)	0.1 (1)	−1.4 (2)
O(3)	4.6 (2)	5.6 (2)	7.2 (2)	1.8 (2)	0.1 (1)	0.3 (2)
O(4)	8.2 (2)	3.3 (2)	6.7 (2)	1.7 (2)	1.2 (2)	0.8 (1)
O(5)	7.1 (2)	7.8 (2)	4.9 (2)	1.8 (2)	2.5 (2)	0.0 (2)
O(6)	7.3 (2)	8.7 (3)	6.3 (2)	−3.0 (2)	−2.4 (2)	−0.7 (2)
O(7)	5.3 (1)	2.3 (1)	2.2 (1)	0.4 (1)	0.5 (1)	0.2 (1)
O(8)	4.1 (1)	2.6 (1)	2.6 (1)	−0.3 (1)	0.0 (1)	0.2 (1)
O(9)	6.3 (2)	2.9 (1)	2.2 (1)	−0.2 (1)	0.7 (1)	0.1 (1)
O(10)	4.8 (1)	3.1 (1)	2.3 (1)	0.3 (1)	0.8 (1)	0.4 (1)
C(1)	5.0 (2)	4.5 (2)	3.7 (2)	−0.4 (2)	−1.0 (2)	0.6 (2)
C(2)	4.0 (2)	4.2 (2)	3.1 (2)	0.3 (2)	−0.5 (2)	−0.2 (2)
C(3)	3.7 (2)	4.0 (2)	3.3 (2)	0.1 (2)	0.2 (2)	0.1 (2)
C(4)	4.5 (2)	3.4 (2)	3.6 (2)	0.8 (2)	0.7 (2)	−0.3 (2)
C(5)	3.8 (2)	4.5 (2)	3.6 (2)	0.9 (2)	0.6 (2)	0.1 (2)
C(6)	4.5 (2)	4.7 (2)	4.1 (2)	−0.6 (2)	−0.3 (2)	−0.1 (2)
C(7)	5.6 (2)	3.0 (2)	2.5 (2)	−0.2 (2)	0.0 (2)	0.1 (1)
C(8)	5.2 (2)	2.8 (2)	2.3 (2)	0.2 (2)	0.2 (2)	0.2 (1)
C(9)	4.8 (2)	3.0 (2)	2.5 (2)	0.1 (2)	−0.1 (2)	0.4 (1)
C(10)	8.4 (3)	4.1 (2)	2.5 (2)	0.6 (2)	−1.2 (2)	−0.2 (2)
C(11)	5.6 (2)	4.4 (2)	3.9 (2)	0.6 (2)	1.5 (2)	0.4 (2)
C(12)	6.0 (2)	3.0 (2)	3.6 (2)	0.6 (2)	1.4 (2)	0.2 (2)
C(13)	4.9 (2)	3.2 (2)	3.1 (2)	0.7 (2)	0.9 (2)	0.5 (1)
C(14)	4.5 (2)	3.7 (2)	3.2 (2)	0.9 (2)	0.2 (2)	0.5 (2)
C(15)	8.9 (4)	4.8 (3)	6.1 (3)	2.9 (3)	2.0 (3)	1.9 (2)
C(16)	6.4 (3)	3.8 (2)	4.3 (3)	−0.6 (2)	1.6 (2)	−0.3 (2)

[a] Hydrogen atom positions were obtained by parabolic interpolation of peaks on a three-dimensional difference Fourier map and were not refined. H(7-1) and H(7-2) are attached to C(7), etc. [b] Anisotropic thermal parameters of the form $\exp[-0.25(B_{11}h^2a^{*2} + B_{22}k^2b^{*2} + B_{33}l^2c^{*2} + 2B_{12}hka^*b^* + 2B_{13}hla^*c^* + 2B_{23}klb^*c^*)]$ were used for all nonhydrogen atoms. Hydrogen atoms were assigned an isotropic thermal parameter of $B = 6.0$ Å^2 which was not refined.

complex, and this interpretation is supported by the observation that the four Fe–C bonds trans to phosphorus (average 1.803 Å) are longer than the other two Fe–C bonds in this molecule (average 1.762 Å). No such differences are seen in the $[(CF_3)_2PFe(CO)_3]_2$ structure. On the other hand, Burdett[3] has found that including the phosphorus 3d orbitals in his calculations on the hypothetical $[F_2PFe(CO)_3]_2$ molecule resulted in increased values for the Fe–Fe distance and the dihedral angle about the P···P line, whereas no particular effect can be seen on these parameters in the $[(\mu\text{-DMP})Fe(CO)_3]_2$ structure.

It is worth noting the relative insensitivity of the P···P distances and P–Fe–P angles to the identity of the substituents on phosphorus (see Table IV). This is another indication that the degree of steric interaction between these substituents is rather small, even for such bulky substituents as CF_3.

The remaining distances and angles within the $[(\mu\text{-DMP})Fe(CO)_3]_2$ molecule are of the expected values. The

Table III. Intramolecular Distances, Angles, and Least Squares Planes

A. Intramolecular Distances, Å

Fe(1)-Fe(2)	2.680 (1)	O(4)-C(4)	1.137 (5)
Fe(1)-P(1)	2.145 (1)	O(5)-C(5)	1.129 (5)
Fe(1)-P(2)	2.195 (1)	O(6)-C(6)	1.145 (5)
Fe(1)-C(1)	1.803 (5)	O(7)-C(7)	1.454 (5)
Fe(1)-C(2)	1.799 (4)	O(8)-C(9)	1.459 (4)
Fe(1)-C(3)	1.763 (4)	O(9)-C(12)	1.446 (5)
Fe(2)-P(1)	2.198 (1)	O(10)-C(14)	1.453 (5)
Fe(2)-P(2)	2.147 (1)	C(7)-C(8)	1.535 (5)
Fe(2)-C(4)	1.798 (4)	C(8)-C(9)	1.522 (5)
Fe(2)-C(5)	1.810 (4)	C(8)-C(10)	1.524 (6)
Fe(2)-C(6)	1.761 (5)	C(8)-C(11)	1.519 (6)
P(1)-O(7)	1.608 (2)	C(12)-C(13)	1.529 (5)
P(1)-O(8)	1.611 (2)	C(13)-C(14)	1.519 (6)
P(2)-O(9)	1.604 (3)	C(13)-C(15)	1.536 (6)
P(2)-O(10)	1.610 (2)	C(13)-C(16)	1.519 (7)
O(1)-C(1)	1.139 (5)	P(1)···P(2)	2.773 (1)
O(2)-C(2)	1.144 (5)	O(7)···O(9)	3.075 (3)
O(3)-C(3)	1.144 (5)		

B. Intermolecular Distances Less Than 3.5 Å

O(6)···C(9)	3.302 (5)	O(3)···C(6)	3.410 (6)
O(1)···O(5)	3.322 (5)	O(5)···C(1)	3.459 (6)
O(2)···O(5)	3.335 (5)	O(2)···O(2)	3.473 (7)
O(2)···C(15)	3.362 (7)	O(4)···C(10)	3.481 (6)

C. Bond Angles, Deg

Fe(2)-Fe(1)-P(1)	52.78 (3)	Fe(2)-P(1)-O(8)	117.0 (1)
Fe(2)-Fe(1)-P(2)	51.09 (3)	O(7)-P(1)-O(8)	102.0 (1)
Fe(2)-Fe(1)-C(1)	108.8 (1)	Fe(1)-P(2)-Fe(2)	76.22 (4)
Fe(2)-Fe(1)-C(2)	96.2 (1)	Fe(1)-P(2)-O(9)	122.5 (1)
Fe(2)-Fe(1)-C(3)	143.0 (1)	Fe(1)-P(2)-O(10)	117.9 (1)
P(1)-Fe(1)-P(2)	79.42 (4)	Fe(2)-P(2)-O(9)	118.2 (1)
P(1)-Fe(1)-C(1)	89.2 (1)	Fe(2)-P(2)-O(10)	120.5 (1)
P(1)-Fe(1)-C(2)	147.0 (1)	O(9)-P(2)-O(10)	101.8 (1)
P(1)-Fe(1)-C(3)	107.6 (1)	P(1)-O(7)-C(7)	117.3 (2)
P(2)-Fe(1)-C(1)	159.8 (1)	P(1)-O(8)-C(9)	116.9 (2)
P(2)-Fe(1)-C(2)	89.1 (1)	P(2)-O(9)-O(10)	119.1 (2)
P(2)-Fe(1)-C(3)	98.4 (1)	P(2)-O(10)-C(12)	116.6 (2)
C(1)-Fe(1)-C(2)	91.6 (2)	Fe(1)-C(1)-O(1)	178.4 (4)
C(1)-Fe(1)-C(3)	101.0 (2)	Fe(1)-C(2)-O(2)	178.6 (4)
C(2)-Fe(1)-C(3)	104.6 (2)	Fe(1)-C(3)-O(3)	178.8 (4)
Fe(1)-Fe(2)-P(1)	51.01 (3)	Fe(2)-C(4)-O(4)	178.1 (4)
Fe(1)-Fe(2)-P(2)	52.69 (3)	Fe(2)-C(5)-O(5)	178.9 (4)

Bond Angles (*Continued*)

Fe(1)-Fe(2)-C(4)	105.9 (1)	Fe(2)-C(6)-O(6)	179.0 (5)
Fe(1)-Fe(2)-C(5)	102.3 (1)	O(7)-C(7)-C(8)	111.5 (3)
Fe(1)-Fe(2)-C(6)	140.4 (2)	C(7)-C(8)-C(9)	108.6 (3)
P(1)-Fe(2)-P(2)	79.31 (4)	C(7)-C(8)-C(10)	108.0 (4)
P(1)-Fe(2)-C(4)	88.3 (1)	C(7)-C(8)-C(11)	111.1 (3)
P(1)-Fe(2)-C(5)	152.1 (1)	C(9)-C(8)-C(10)	107.2 (3)
P(1)-Fe(2)-C(6)	102.6 (2)	C(9)-C(8)-C(11)	110.8 (3)
P(2)-Fe(2)-C(4)	158.5 (1)	C(10)-C(8)-C(11)	111.1 (4)
P(2)-Fe(2)-C(5)	90.4 (1)	O(8)-C(9)-C(8)	111.3 (3)
P(2)-Fe(2)-C(6)	98.5 (2)	O(9)-C(12)-C(13)	111.5 (3)
C(4)-Fe(2)-C(5)	92.6 (2)	C(12)-C(13)-C(14)	108.3 (3)
C(4)-Fe(2)-C(6)	101.3 (2)	C(12)-C(13)-C(15)	106.3 (3)
C(5)-Fe(2)-C(6)	104.6 (2)	C(12)-C(13)-C(16)	112.2 (4)
Fe(1)-P(1)-Fe(2)	76.21 (3)	C(14)-C(13)-C(15)	108.2 (4)
Fe(1)-P(1)-O(7)	122.0 (1)	C(14)-C(13)-C(16)	110.3 (3)
Fe(1)-P(1)-O(8)	117.9 (1)	C(15)-C(13)-C(16)	111.4 (4)
Fe(2)-P(1)-O(7)	121.8 (1)	O(10)-C(14)-C(13)	112.0 (3)

D. Least-Squares Planes

I. Plane through Fe(1), Fe(2), P(1)
$1.081x + 9.735y - 0.067z = 3.388$

II. Plane through Fe(1), Fe(2), P(2)
$-2.311x + 3.528y + 26.177z = 10.582$

III. Plane through Fe(1), P(1), P(2)
$-4.916x + 7.398y + 6.685z = 2.895$

IV. Plane through Fe(2), P(1), P(2)
$3.692x + 5.710y + 19.101z = 9.302$

V. Plane through P(1), O(7), O(8)
$7.283x - 1.203y + 9.868z = 5.282$

VI. Plane through P(2), O(9), O(10)
$7.344x - 1.735y + 8.547z = 4.600$

VII. Plane through P(1), P(2), O(7), O(8), O(9), O(10)
$7.250x - 1.604y + 9.712z = 5.083$

Perpendicular Distances from Plane VII, Å

P(1)	0.010	P(2)	−0.014
O(7)	0.065	O(9)	0.065
O(8)	−0.038	O(10)	0.042

Dihedral Angles between Planes, Deg

I-II	108.5	V-VI	176.0
III-IV	106.6		

Table IV. Structural Features of $[R_2PFe(CO)_3]_2$ Complexes

	R = H, CH_3, C_6H_5[a]			
	Range	Av of 5 complexes	R = alkoxy[b]	R = CF_3[c]
Fe-Fe, Å	2.619-2.665	2.646	2.680	2.819
Fe-P, Å	2.203-2.233	2.215	2.171 (av)	2.193
P···P, Å	2.725-2.925	2.834	2.773	2.921
Fe-P-Fe, deg	72.0-74.3	73.4	76.2 (av)	80.0
P-Fe-P, deg	76.4-82.9	79.6	79.4 (av)	83.5
Dihedral angles, deg				
About P···P	100.0-107.3	102.2	106.6	118.9
About Fe-Fe	101.8-112.2[c]	105.9[c]	108.5	120.8

[a] J. R. Huntsman and L. F. Dahl, to be submitted for publication (quoted in ref 2). [b] This study. [c] Calculated from data quoted in ref 2.

Fe–CO systems are all essentially linear.

The Structure and Fluxonality of $[(\mu\text{-DMP})Fe(CO)_3]_2$. One reason for determining the structure of $[(\mu\text{-DMP})Fe(CO)_3]_2$ was to evaluate possible reasons for the high degree of fluxionality of this molecule and in particular for the comparative ease of inversion of its Fe_2P_2 ring, a process which exhibits a coalescence temperature below those shown by other $[R_2PFe(CO)_3]_2$ complexes.[1] It is possible, on the basis of structural data, to examine two possibilities: that this efect is due to steric interaction between the phosphorinane rings or that it is the result of the electronic properties of the alkoxy substituents on the phosphorus atoms.

The first of these possibilities, that steric repulsion between the phosphorinane rings forces the phosphorus atoms apart, flattens the Fe_2P_2 ring, and lowers the barrier to inversion, would seem to be straightforwardly eliminated on the basis of the observed structure. This is no evidence to show such repulsion; the P···P distance is, if anything, nearer the short end of the range observed in $[R_2PFe(CO)_3]_2$ complexes, and there is no appreciable distortion of the two PO_2 planes away from coplanarity as would be expected if the two rings were impinging upon one another.

The hypothesis that the ease of inversion of the Fe_2P_2 ring is an effect of the electronic properties of the substituents on the phosphorus atoms is more difficult to evaluate. However, there seems to be little evidence in the observed structure of $[(\mu\text{-DMP})Fe(CO)_3]_2$ to support it. Most of the structural parameters of the Fe_2P_2 system in this molecule, and particularly those most relevant to the ring inversion process (namely, the Fe–Fe bond length and the dihedral angle about the Fe–Fe bond), are intermediate between those found in, say, $[(CH_3)_2PFe(CO)_3]_2$ and $[(CF_3)_2PFe(CO)_3]_2$. However, the coalescence temperature for Fe_2P_2 ring inversion in $[(\mu\text{-DMP})Fe(CO)_3]_2$ (55–60 °C) is well below those for both of the other compounds.[7,8] There is then no correlation between the ease of ring inversion and these structural parameters, nor is there a correlation with the electronegativities of the phosphorus substituents insofar as they are reflected in these parameters.

There remains the possibility that Fe_2P_2 ring inversion in $[(\mu\text{-DMP})Fe(CO)_3]_2$ is influenced by enhanced Fe–P $d\pi$–$d\pi$ bonding. If such π bonding is important and if it does influence the inversion process, it does so without any apparent structural consequences (apart from the short Fe–P and long Fe–C bonds). The question of whether this is possible cannot be resolved by a purely structural investigation. However, Burdett[3] has argued that the equilibrium geometry in $[R_2PFe(CO)_3]_2$ complexes results largely from a balance between Fe–P and Fe–Fe interactions. It seems very unlikely that any electronic effect sufficient to influence the inversion rate (by altering the relative energies of the molecular orbitals so as to reduce the barrier to inversion) would fail to affect these interactions and thus the molecular geometry as well.

Thus it appears, as has been suggested earlier,[1] that neither steric nor electronic effects seem to provide a satisfactory explanation for the relative ease of inversion of the Fe_2P_2 ring in $[(\mu\text{-DMP})Fe(CO)_3]_2$. This strengthens our confidence in the hypothesis that the rate of this process is enhanced by coupling with the more rapid inversion of the phosphorinane ring.[1] However, it is not possible to evaluate this possibility using static structural data; this will require further NMR studies of other compounds.

Acknowledgment. This work was supported by the assistance of the Emory University Computing Center. The authors thank Dr. J. A. Bertrand of Georgia Institute of Technology for generously providing access to his facilities.

Registry No. $[(\mu\text{-DMP})Fe(CO)_3]_2$, 65150-25-6.

Supplementary Material Available: Listing of structure factor amplitudes (18 pages). Ordering information is given on any current masthead page.

References and Notes

(1) C. M. Bartish and C. S. Kraihanzel, *Inorg. Chem.*, **17**, 735 (1978).
(2) W. Clegg, *Inorg. Chem.*, **15**, 1609 (1976).
(3) J. K. Burdett, *J. Chem. Soc., Dalton Trans.*, 423 (1977).
(4) R. J. Doedens and J. A. Ibers, *Inorg. Chem.*, **6**, 204 (1967).
(5) "International Tables for X-ray Crystallography", Vol. IV, Kynoch Press, Birmingham, England, 1974: (a) pp 72–98; (b) pp 149–150.
(6) P. M. Treichel, W. K. Dean, and J. L. Calabrese, *Inorg. Chem.*, **12**, 2908 (1973).
(7) R. E. Dessy, A. L. Rheingold, and G. D. Howard, *J. Am. Chem. Soc.*, **94**, 746 (1972).
(8) J. Grobe, *Z. Anorg. Allg. Chem.*, **361**, 32 (1968).

Contribution from the Department of Chemistry, University of South Carolina, Columbia, South Carolina 29208

Crystal and Molecular Structure of a Colored Intermediate from the Reaction of Tetramethylthiourea and Copper(2+) (Dichlorobis(tetramethylthiourea)copper(II))

E. A. H. GRIFFITH, W. A. SPOFFORD, III, and E. L. AMMA*

Received July 28, 1977

The crystal and molecular structure of dichlorobis(tetramethylthiourea)copper(II) has been determined. The structure consists of isolated molecules separated by ordinary van der Waals distances. The environment of the metal atom is that of a distorted tetrahedron with Cu–Cl distances of 2.241 (6) and 2.234 (6) Å and Cu–S distances of 2.314 (7) and 2.316 (6) Å. The Cl–Cu–Cl angle is 145.0 (3)° and the S–Cu–S angle is 140.1 (3)° while the Cl–Cu–S angles are 98° or less. The orientation of the tetramethylthiourea groups is determined by chlorine–methyl replusions. The tetramethylthiourea group is distorted from planarity due to methyl–methyl interference. A consistent reaction scheme and structure relationship is proposed including this intermediate and related intermediates as well as the structurally diverse reaction products of thiourea and cupric ion in aqueous solution. The crystals are monoclinic: $P2_1$; $a = 9.464$ (2), $b = 8.550$ (1), $c = 11.532$ (2) Å; $\beta = 105.56$ (4)°; $\rho_o = 1.46$, $\rho_c = 1.47$ g cm^{-3}; $Z = 2$. The structure was solved by standard heavy-atom methods and refined by full-matrix least squares including anisotropic temperature factors to an R of 0.064 with 1133 reflections.

Introduction

In the reaction of thiourea $[SC(NH_2)_2]$, tu, with metal ions, such as Fe^{3+} or Cu^{2+}, which are capable of setting up a redox system in aqueous solution, transient intermediates of unusual color are frequently observed.[1] In particular, Cu^{2+} with thiourea and substituted thioureas gives a rose to purple transient intermediate in which the exact color is dependent upon the thiourea derivative and is especially anion dependent. These colored intermediates may further react to a series of polynuclear Cu(I) intermediates such as $Cu_4S_6^{4+}$, $Cu_4S_9^{4+}$ [2] (S = a particular thiourea ligand) which ends in an infinite polymer $(Cu_4S_9^{4+})_x$.[3] Alternatively these colored intermediates may proceed directly to the following: polymeric end products such as $(Cu_4S_{10}^{4+})_x$[4] which contain Cu–S bridged six-membered Cu_3S_3 rings; linear Cu–S bridged polymers $(CuS_2Cl)_x$;[5] Cu–S bridged dimers such as $Cu_4S_6^{2+}$;[6,7] isolated planar three-coordinate Cu(I) entities, CuS_3^+,[8] or isolated tetrahedral Cu(I) moieties, CuS_3Cl[9] (for details vide infra). The exact end product is dependent upon steric factors and concentration of the sulfur ligand as well as the anion. With the ligand tetramethylthiourea, the chloride anion, and Cu^{2+} we have been able to isolate the colored intermediate and preserve a few crystals for a sufficient period of time to carry out a single-crystal structure analysis. We wish to report the details[10] of that analysis here and relate the structure of this intermediate to the known structures of many of the reaction products of this process.

Experimental Section

Preparation. Tetramethylthiourea (1.3 g (0.01 mol) in 60 mL of H_2O) was mixed with approximately 1 L of crushed ice. A deep burgundy color developed as soon as $CuCl_2 \cdot 2H_2O$ [0.4 g (0.0023 mol) in 400 mL of H_2O] was added slowly with rapid stirring. The color gradually faded to colorless (~2 h) and the solution was maintained thereafter at room temperature. After 2 days a small amount of free sulfur was filtered off and the solution was allowed to evaporate almost to dryness. A reddish brown oil developed in which ruby red crystals formed in large clumps or aggregates. Diffraction-grade fragments were immediately cleaved from these clumps since the crystalline material is unstable if allowed to remain in the oil or left in contact with open air. Accordingly, a number of samples were coated with petroleum jelly and sealed in Lindemann capillaries for diffraction studies.

X-Ray Data. Preliminary Weissenberg and precession photographic data showed that the crystals were monoclinic with systematic absences of $k = 2n + 1$ for $0k0$, which is compatible for either space group

0020-1669/78/1317-1913$01.00/0